# Determination of surface complex nonlinear optical susceptibilities and molecular orientational distribution functions using resonant surface second-harmonic generation

Byoungchoo Park, Jeong-Geun Yoo, Takahiro Sakai, Hajime Hoshi, Ken Ishikawa, and Hideo Takezoe
*Department of Organic and Polymeric Materials, Tokyo Institute of Technology, O-okayama, Meguro-ku, Tokyo 152-5882, Japan*
(Received 27 April 1998)

Using the resonant optical surface second-harmonic generation (SHG), we have determined the relative values of the complex nonlinear optical (NLO) components ($\chi_{zzz}$, $\chi_{zxx}$, and $\chi_{xxz}$) at isotropic interfaces ($C_{\infty v}$) of a polymer with SHG active side chains. The introduced configuration of the SHG experiment was a polarizer–rotating quarter wave plate–sample–analyzer. It was shown that this configuration gives information on complex NLO coefficients without using the Kleinmann symmetry. For the experiments, we measured resonant surface SHG from the air-polymer and the substrate-polymer interfaces of a thick polymer film. By theoretically fitting the SHG data, we unambiguously determined the nonlinear susceptibility components at the both interfaces of the polymer film. Moreover, unbiased molecular orientational distribution functions (ODFs) at both interfaces were also determined using the modified maximum entropy method. The obtained ODFs were found to be quite different from the previous ones obtained by assuming the Kleinmann symmetry, indicating the important role of the imaginary part of $\chi$'s played when determining ODFs.
[S1063-651X(98)02210-7]

PACS number(s): 68.45.−v, 61.30.−v, 64.70.−p, 42.65.Ky

## I. INTRODUCTION

It is well known that molecular ordering at a surface or an interface may be significantly different from that in the bulk. The molecular surface ordering is a problem not only of fundamental interest, but also of practical importance for fabricating organic devices such as liquid crystal (LC) displays [1–14]. In the past few years, many kinds of optical methods have been proposed in order to obtain information about molecular ordering at surfaces [3–5]. Among them, optical second-harmonic generation (SHG) has proved to be a sensitive tool for studying the polar arrangement of adsorbed molecular layers [5–14]. Up to now, the surface SHG measurement has been widely applied to various kinds of organic systems such as LC molecules on alignment layers [9–11,13,14], polymer monolayers [15], and spin-coated films of polymer possessing SHG active side chains [12,13,16,17]. In these SHG measurements, the polarizer-sample-analyzer configuration has been usually used to obtain the surface nonlinear optical (NLO) coefficients. With these NLO coefficients, one could deduce the molecular orientational distribution functions (ODFs) at surfaces or interfaces [9–18].

Until now, most surface SHG has been measured under optical resonance conditions because the generated signal level is too low to detect it at the off-resonance condition [5–17]. Two serious problems arise in the theoretical analysis for the surface SHG results under a resonant condition. The first is the contribution of imaginary parts of NLO coefficients to the SHG intensity and the second is the invalidity of the Kleinmann symmetry for the NLO coefficients. If these problems are taken into account, the number of unknown NLO coefficients increases. Hence one needs independent sets of experimental data sufficient to obtain the values of NLO coefficients. However, the theoretical analysis using the traditional polarizer-sample-analyzer configuration does not allow one to obtain all of the complex NLO coefficients without assuming the Kleinmann symmetry under resonant conditions because the number of SHG data sets is restricted by the four combinations of polarization states for the polarizer and the analyzer. Thus, to analyze the SHG results, one usually assumes the real-valued NLO coefficients and the validity of the Kleinmann symmetry even under resonance conditions. Because of these assumptions, the molecular ODF deduced from the NLO coefficients is not fully reliable.

Recently, the quarter wave plate (QWP)–sample–analyzer configurations have been suggested for the study of chiral [19,20] and nonchiral [21] surfaces. These configurations show a possibility to obtain the complex NLO coefficients, although the direct application of its theoretical analysis to nonchiral surfaces is not suitable to obtain the direct information about the surfaces such as the ratio of the imaginary part and real part of the NLO coefficients.

In this study, to overcome these restrictions, we propose a polarizer–rotating QWP–sample geometry–analyzer configuration. It is demonstrated that one can determine the relative values of all the complex NLO coefficients of interfaces with $C_{\infty v}$ symmetry without assuming the Kleinmann symmetry under resonance conditions. Together with the complex NLO coefficients, the molecular ODFs at the interfaces were also obtained using the modified maximum entropy method.

## II. THEORETICAL BACKGROUND

The surface SHG signal is proportional to the square of the effective second-order surface NLO susceptibility $\chi^{(2)}_{\mathrm{eff}}$ [5–8]. For the case of azimuthally isotropic surfaces ($C_{\infty v}$ symmetry), there are three independent nonvanishing NLO components, i.e., $\chi_{zzz}$, $\chi_{zxx}$, and $\chi_{xxz}$. In most of the papers, $\chi_{zxx}$ was assumed to be equal to $\chi_{xxz}$ (Kleinmann symmetry) and moreover the imaginary part of these two inde-

 

pendent components ($\chi_{zzz}$ and $\chi_{zxx}$) was neglected. In the present paper the three complex components are treated independently. Then the surface SHG signals are described by the three complex NLO coefficients under resonant conditions.

Let us consider the polarizer–rotating QWP–optical sample geometry (reflection and transmission)–analyzer configuration, which is shown in Fig. 1(a). The rotating QWP was used to continuously vary the relative phase and amplitude of the electric field components of a fundamental beam. The rotating angle of the QWP is defined by the angle $\Phi$ between the fast axis of the QWP and the *s*-polarized direction. When the polarization direction of the polarizer is set to *p* polarization, the unit vector of the electric field for the incident fundamental beam at the SHG active layer after passing through the QWP is given by $(i\cos^2\Phi+\sin^2\Phi)\cos\theta_{\rm in}$, $(i\cos^2\Phi+\sin^2\Phi)\sin\theta_{\rm in}$, and $(1-i)\cos\Phi\sin\Phi$, where $\theta_{\rm in}$ and $\theta_{\rm out}$ are the angles of refraction at the layer for the propagating fundamental and SHG waves, respectively. When the polarization direction of the polarizer is set to *s* polarization, the unit vector of the fundamental electric field after the QWP is given by $(1-i)\cos\Phi\sin\Phi\cos\theta_{\rm in}$, $\cos^2\Phi+i\sin^2\Phi$, and $(1-i\cos\Phi\sin\Phi\sin\theta_{\rm in})$. If the surface second harmonic (SH) beam propagates to the reflected directions, then the unit vectors of the SHG electric field are written $(-\cos\theta_{\rm out}, 0, \sin\theta_{\rm out})$ for the *p* polarization and (0, 1, 0) for the *s* polarization. On the other hand, for the transmitted SH beam, the unit vectors of the electric field are given by $(\cos\theta_{\rm out}, 0, \sin\theta_{\rm out})$ for the *p* polarization and (0, 1, 0) for the *s* polarization. Thus we can obtain the eight combinations of the effective NLO susceptibilities for the polarizer (*p* or *s*)–QWP–sample (*r* for reflection or *t* for transmission)–analyzer (*p* or *s*) configuration. The eight effective NLO susceptibilities can be written

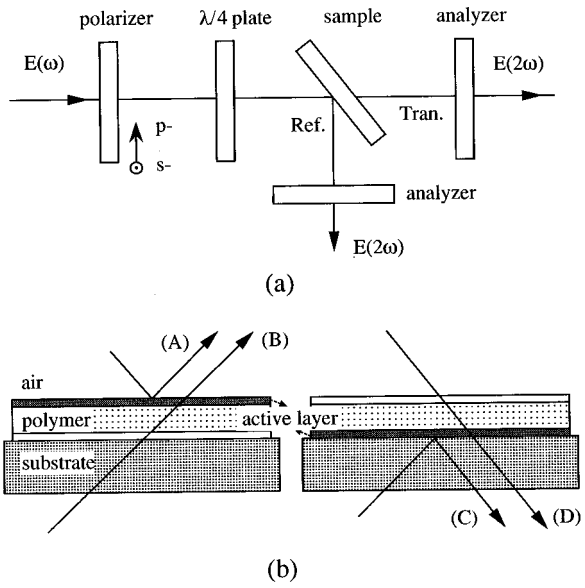


FIG. 1. (a) Configuration of polarizer–quarter wave plate–sample–analyzer. (b) Four kinds of sample geometries: (*A*) air-reflection, (*B*) air-transmission, (*C*) substrate-reflection, and (*D*) substrate-transmission.

$$\chi^{(2)}_{{\rm eff},prp}=-2L(2\omega)_xL(\omega)_xL(\omega)_z\chi_{xxz}(i\cos^2\Phi+\sin^2\Phi)^2\cos\theta_{\rm in}\sin\theta_{\rm in}\cos\theta_{\rm out}+L(2\omega)_zL(\omega)_x^2\chi_{zxx}(i\cos^2\Phi+\sin^2\Phi)^2\cos^2\theta_{\rm in}\sin\theta_{\rm out}+L(2\omega)_zL(\omega)_z^2\chi_{zzz}(i\cos^2\Phi+\sin^2\Phi)^2\sin^2\theta_{\rm in}\sin\theta_{\rm out}-2iL(2\omega)_zL(\omega)_y^2\chi_{zxx}\cos^2\Phi\sin^2\Phi\sin\theta_{\rm out},\tag{1}$$

$$\chi^{(2)}_{{\rm eff},prs}=2L(\omega)_yL(\omega)_zL(2\omega)_y(1-i)\chi_{xxz}(i\cos^2\Phi+\sin^2\Phi)\cos\Phi\sin\Phi\sin\theta_{\rm in},\tag{2}$$

$$\chi^{(2)}_{{\rm eff},ptp}=2L(2\omega)_xL(\omega)_xL(\omega)_z\chi_{xxz}(i\cos^2\Phi+\sin^2\Phi)^2\sin\theta_{\rm in}\cos\theta_{\rm in}\cos\theta_{\rm out}+L(2\omega)_zL(\omega)_x^2\chi_{zxx}(i\cos^2\Phi+\sin^2\Phi)^2\cos^2\theta_{\rm in}\sin\theta_{\rm out}+L(2\omega)_zL(\omega)_z^2\chi_{zzz}(i\cos^2\Phi+\sin^2\Phi)^2\sin^2\theta_{\rm in}\sin\theta_{\rm out}-2iL(2\omega)_zL(\omega)_y^2\chi_{zxx}\cos^2\Phi\sin^2\Phi\sin\theta_{\rm out},\tag{3}$$

$$\chi^{(2)}_{{\rm eff},pts}=2L(\omega)_yL(\omega)_zL(2\omega)_y(1-i)\chi_{xxz}(i\cos^2\Phi+\sin^2\Phi)\cos\Phi\sin\Phi\sin\theta_{\rm in},\tag{4}$$

$$\chi^{(2)}_{{\rm eff},srp}=4iL(2\omega)_xL(\omega)_xL(\omega)_z\chi_{xxz}\cos^2\Phi\sin^2\Phi\cos\theta_{\rm in}\sin\theta_{\rm in}\cos\theta_{\rm out}-2iL(2\omega)_zL(\omega)_x^2\chi_{zxx}\cos^2\Phi\sin^2\Phi\cos^2\theta_{\rm in}\sin\theta_{\rm out}+L(2\omega)_zL(\omega)_y^2\chi_{zxx}(\cos^2\Phi+i\sin^2\Phi)^2\sin\theta_{\rm out}-2iL(2\omega)_zL(\omega)_z^2\chi_{zzz}\cos^2\Phi\sin^2\Phi\sin^2\theta_{\rm in}\sin\theta_{\rm out},\tag{5}$$

$$\chi^{(2)}_{{\rm eff},srs}=2L(2\omega)_yL(\omega)_yL(\omega)_z(1-i)\chi_{xxz}(\cos\Phi^2+i\sin\Phi^2)\cos\Phi\sin\Phi\sin\theta_{\rm in},\tag{6}$$

$$\chi^{(2)}_{{\rm eff},stp}=-4iL(2\omega)_xL(\omega)_xL(\omega)_z\chi_{xxz}\cos^2\Phi\sin^2\Phi\cos\theta_{\rm in}\sin\theta_{\rm in}\cos\theta_{\rm out}-2iL(2\omega)_zL(\omega)_x^2\chi_{zxx}\cos^2\Phi\sin^2\Phi\cos^2\theta_{\rm in}\sin\theta_{\rm out}+L(2\omega)_zL(\omega)_y^2\chi_{zxx}(\cos^2\Phi+i\sin^2\Phi)^2\sin\theta_{\rm out}-2iL(2\omega)_zL(\omega)_z^2\chi_{zzz}\cos^2\Phi\sin^2\Phi\sin^2\theta_{\rm in}\sin\theta_{\rm out},\tag{7}$$

$$\chi^{(2)}_{{\rm eff},sts}=2L(2\omega)_yL(\omega)_yL(\omega)_z(1-i)\chi_{xxz}(\cos^2\Phi+i\sin^2\Phi)\cos\Phi\sin\Phi\sin\theta_{\rm in},\tag{8}$$

where $L(\Omega)_i$'s ($i=x$, $y$, and $z$) are the local field factors at a frequency of $\Omega$ and generally depend on optical geometries. Equations (2) and (4) and Eqs. (6) and (8) are equivalent. As shown in the above equations, $\chi_{\rm eff}^{(2)}$'s strongly depend on the angle $\Phi$. Therefore, measuring the surface SHG intensities as a function of $\Phi$ for the different polarizer combinations and fitting the obtained SHG data to the above corresponding expressions of $\chi_{\rm eff}^{(2)}$ with appropriate Fresnel factors allow one to calculate the three complex NLO coefficients.

Usually NLO coefficients and molecular ODFs are deduced by separate theoretical fitting procedures, i.e., first the NLO coefficients were determined by the SHG results and the ODFs were deduced using these NLO coefficients. In this study, we combined the two fitting processes to obtain NLO coefficients and ODFs at the same time because the two processes are mutually correlated through the dielectric constants in SHG active layers. For the purpose, the local field corrections for the active layer were made by considering the dielectric constants, which were deduced by taking into account the ODF of the SHG active side chains [17]. Furthermore, an additional constraint function was introduced to get rid of the lack of information on the axial nonpolar ordering when using the maximum entropy method to determine ODFs, i.e., the modified maximum entropy method [18]. These two pieces of the improvement in determining ODFs have already been combined to obtain the anisotropic dielectric constants, the NLO constants, and the ODFs of the SHG active layers, although the effect of the imaginary part of the NLO coefficients and the invalidity of the Kleinmann symmetry were not taken into account [22]. In our fitting procedure, seven constraint functions were used:

$$
\begin{aligned}
f_1(\theta,\phi) &= \cos^3\theta,\\
f_2(\theta,\phi) &= \sin^3\theta\,\cos^3\phi,\\
f_3(\theta,\phi) &= (\cos\,\theta-\cos^3\theta)(1-\cos^2\phi),\\
f_4(\theta,\phi) &= (\cos\,\theta-\cos^3\theta)\cos^2\phi,\\
f_5(\theta,\phi) &= (\sin\,\theta-\sin^3\theta)\cos\,\phi,\\
f_6(\theta,\phi) &= \sin^3\theta(\cos\,\phi-\cos^3\phi),\\
f_7(\theta,\phi) &= (3\cos^2\theta-1)/2.
\end{aligned}
\tag{9}
$$

Here $f_2$, $f_5$, and $f_6$ are zero in $C_{\infty v}$ symmetry and $f_7$ is the additional constraint to introduce the information of axial nonpolar order parameter for the maximum entropy method [18]. For the fitting four undetermined multipliers $\lambda_i$ ($i=1,3,4,7$) were used as fitting parameters for the experimental SHG data with Eqs. (1)–(8). As the result, we obtain the anisotropic dielectric constants, all the complex $\chi_{ijk}$, and the ODFs of the SHG active layers.

## III. EXPERIMENTAL PROCEDURE

The SHG signals were generated using the frequency-doubled output at a wavelength of 532 nm of a *Q*-switched Nd:YAG pulsed laser (where YAG denotes yttrium aluminum garnet). The incident fundamental beam was directed onto the sample at an incidence angle of 45° ($\theta_0$). The polarization state of the fundamental beam was controlled by rotating a QWP after selecting the *p* or *s* polarization of the incident beam. The reflected or transmitted SHG output (266 nm) was selected using an interference filter for both *p* and *s* polarizations.

The polymer used in this experiment was polyimide (PI) with cyanobiphenyl-substituted side chains, which give rise to second-order nonlinear activity, whose structure and optical properties are shown in Refs. [16,17]. The optical absorption peak of the PI film was observed at 288 nm. For the PI film spin coated on a fused quartz substrate, the bulk polymer film does not generate a SH signal because of the random orientation of the side chains. However, the side chains at the air-PI and substrate-PI interfaces can generate a SH signal because of their polar orientations [16,17]. Thus the film sample can be described as a system consisting of the SHG active air-PI interface, the SHG inactive bulk film, and the SHG active substrate-PI interface. To distinguish the SHG signals from the two interfaces, we prepared thick (about 740 nm) PI films whose optical density was more than 3 at the SHG wavelength (266 nm). The high optical density ensures that the SHG light from the rear interface with respect to the detector is completely absorbed during the propagation in the bulk film and cannot be detected. Thus the SHG from the two interfaces can be selectively observed. For the study of the air-PI interface, we used the air-reflection (*A*) and air-transmission (*B*) sample geometries, as shown in Fig. 1(b). For the study of the substrate-PI interface, we used the substrate-reflection (*C*) and substrate-transmission (*D*) sample geometries.

## IV. RESULTS AND DISCUSSION

Now we describe the surface SHG results for the polymer film. Figures 2(a) and 2(b) show the SHG intensity profiles as a function of $\Phi$ for the eight configurations from the air-PI and substrate-PI interfaces, respectively. The four-letter labels of data in the figure such as ''*parp*'' represents the polarization state of the polarizer (*p* or *s*), the interfaced medium [*a* for air or *g* for glass (fused quartz) substrate], the optical geometry (*r* for reflection or *t* for transmission), and the polarization state of the analyzer (*p* or *s*). As shown in Fig. 2, the SHG intensity profiles show the characteristic line shapes. It is noted that the SHG intensities from the substrate-PI interface are smaller than those from the air-PI interface. In order to determine the values of $\chi_{zzz}$, $\chi_{zxx}$, and $\chi_{xxz}$ of each interface, we fitted the obtained SHG results to the theoretical expressions using the fitting procedure mentioned above for each interface. In this fitting procedure, the fitting routines for the air-PI [Fig. 2(a)] and substrate-PI [Fig. 2(b)] interfaces were combined to obtain NLO coefficients and ODFs at each interface simultaneously because the SHG results of each interface are mutually affected by the other interface in terms of the dielectric constants and the boundary conditions for transmission and reflection of the fundamental and SHG fields. Only relative values of the coefficients need to be known and so we normalize $\mathrm{Re}(\chi_{zzz})=1$ for the air-PI interface. From the best fit, we could obtain the theoretical SHG intensity profiles, as shown in Fig. 2 (solid curves). It is clear that the theoretical SHG intensity profiles fit very well with the experimental results within the experi-

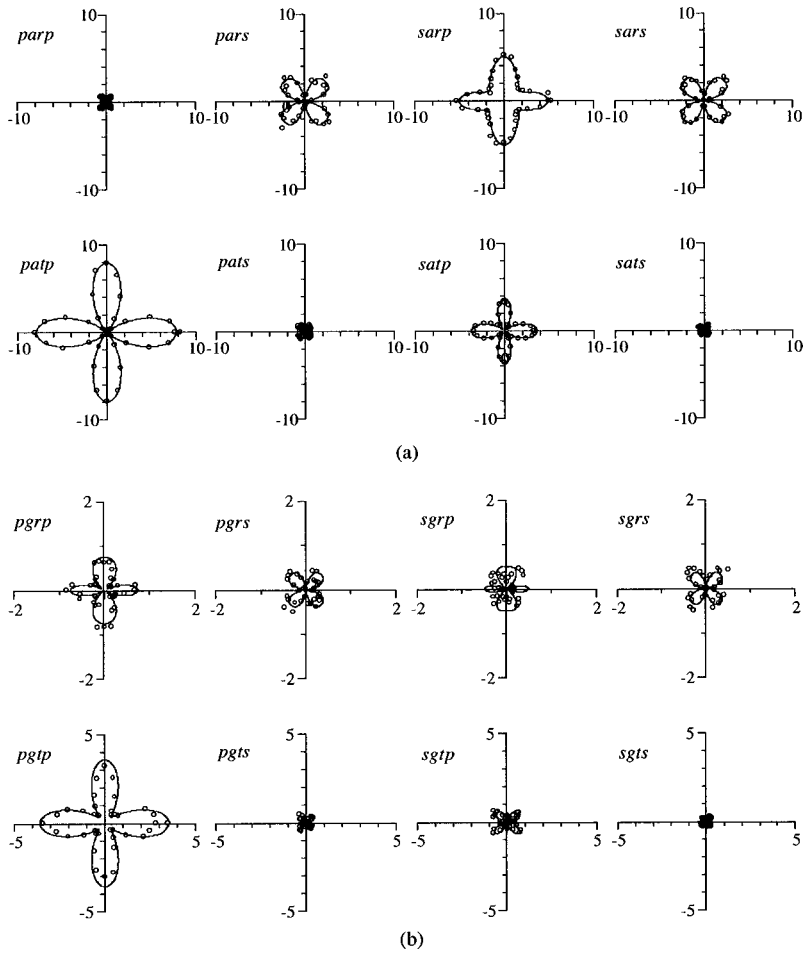


FIG. 2. (a) SHG intensities (circles) from the air-PI interface as a function of $\Phi$ using the *A* and *B* geometries. (b) SHG intensities (circles) from the substrate-PI interface as a function of $\Phi$ using the *C* and *D* geometries. The best-fit results are shown by solid curves.

mental errors. The obtained ratios of the complex NLO coefficients are $\chi_{zzz}:\chi_{zxx}:\chi_{xxz}=1.00+i0.13:0.11+i0.01:0.12+i0.02$ for the air-PI interface and $\chi_{zzz}:\chi_{zxx}:\chi_{xxz}=23.84+i3.03:2.53+i0.33:2.84+i0.36$ for the substrate-PI interface. According to this fitted result, the imaginary parts of the NLO coefficients are approximately 13% and $\chi_{xxz}$ is slightly larger than $\chi_{zxx}$ by 12%. In the present treatment, the standard deviation for the best fitting was $7.95\times10^{-3}$, while that without considering the imaginary part was $8.79\times10^{-2}$. This indicates the importance of considering the imaginary part.

Next we describe the surface ODFs of the SHG active side chains at both interfaces of the polymer film. It was assumed that the side chain is a rodlike molecule whose second-order hyperpolarizability is dominated by a single element $\beta_{\xi\xi\xi}$ along the molecular long axis $\xi$ [5–8]. In the calculation of ODFs, we used the obtained ratio of $\chi_{zzz}/\chi_{zxx}$ because of the small difference between $\chi_{zxx}$ and $\chi_{xxz}$. With the ratios of NLO coefficients for the two interfaces, we obtained the ODFs $f_a$ and $f_g$ of the side chains at the air-side and the substrate-side active layers, respectively. The distributions $f_a$ and $f_g$ are plotted in Fig. 3 as a function of $\theta$ since they are isotropic with respect to the azimuth angle $\phi$. The distribution $f_a$ exhibits two broad peaks for the tilt (polar) angle $\theta$ at $\theta=0°$ and 180°, while the distribution $f_g$ exhibits only one broad peak at $\theta=0°$. The proportion of molecules between $\theta=90°$ and 180° in the distribution $f_a$ is approximately 46.0%, while that in the distribution $f_g$ is zero. At this moment, we cannot define the directional sense, namely, whether $\theta=0°$ is defined toward the outside of the polymer film or toward the inside of the polymer film. For the deter-

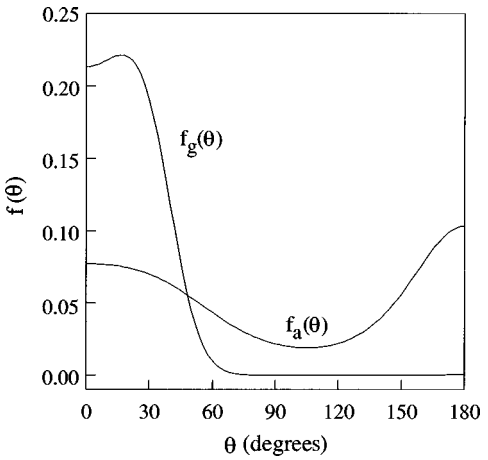


FIG. 3. Orientation distribution functions of the side chains: the distribution $f_a$ at the air-PI interface and the distribution $f_g$ at the PI-substrate interface.

mination, SHG interferometry measurements are necessary. In order to estimate the ordering of the side chain at the interface, we calculated the surface order parameters $\langle \cos\theta \rangle$ and $\langle \cos^2\theta \rangle$, which correspond to the polar and axial order parameters, respectively, with respect to the surface normal direction ($z$). For the distribution $f_a$, i.e., the air-PI interface, the obtained $\langle \cos\theta \rangle$ is 0.01 and $\langle \cos^2\theta \rangle$ is 0.54. Thus the side chains at the air-PI interface are axially ordered with respect to $z$, though the polar ordering is weak. On the other hand, the side chains at the substrate-PI interface take an upright position due to the strong polar interaction between the side chain and the substrate. For the substrate-PI interface, $\langle \cos\theta \rangle$ is 0.90 and $\langle \cos^2\theta \rangle$ is 0.81. From the comparison of the surface order parameters, it is clear that the side chains at the substrate-PI interface are more highly polar and axially ordered than those at the air-PI interface.

Finally, we want to comment on the hyperpolarizability $\beta_{\xi\xi\xi}$ of the side-chain molecules. From the ratios of the NLO coefficients with the order parameters calculated from the molecular ODFs, we could deduce that the ratio of $\mathrm{Im}(\beta_{\xi\xi\xi})$:$\mathrm{Re}(\beta_{\xi\xi\xi})$ is 0.13. The ratio obtained from $C_{\infty v}$ symmetry could be used to analyze the more complicated systems, for example, the $C_{1v}$ symmetry system such as the rubbed surface of the LC alignment layer.

## V. CONCLUSIONS

In summary, the measurements of the surface SHG using the polarizer–QWP–sample–analyzer configuration together with the analysis using the modified maximum entropy method have led us to determine unambiguously the ratios of the complex NLO coefficients and ODFs at interfaces. The results for the interfaces of polymer film indicate that highly polar surface orientation is formed at the substrate-PI interface. In contrast, there exist two orientations pointing away from the polymer and toward inside of the polymer at the air-PI interface, resulting in less polar orientation. These orientations have not been obtained under the assumption of Kleinmann symmetry, indicating the serious influence of the imaginary part of the $\chi$ components under resonant conditions in determining the ODF. Both the optical technique and the theoretical analysis for this configuration can be easily generalized to the study of various organic surfaces and interfaces such as LC molecules on the alignment layer, polymer interfaces, and Langmuir-Blodgett films.

## ACKNOWLEDGMENT

B.P. was supported by the Korea Science & Engineering Foundation (KOSEF).

[1] J. S. Foster and J. E. Frommer, Nature (London) **333**, 542 (1988).
[2] D. P. E. Smith, H. Horber, C. Gerber, and B. Binnig, Science **245**, 43 (1989).
[3] T. J. Sluckin and A. Poniewierski, *Fluid Interfacial Phenomena* (Wiley, New York, 1986), Chap. 5, and references therein.
[4] W. Chen, L. J. Martinez-Miranda, H. Hsiung, and Y. R. Shen, Phys. Rev. Lett. **62**, 1860 (1989).
[5] Y. R. Shen, Annu. Rev. Phys. Chem. **40**, 327 (1989).
[6] W. Chen, M. B. Feller, and Y. R. Shen, Phys. Rev. Lett. **63**, 2665 (1989).
[7] Y. R. Shen, Nature (London) **337**, 519 (1989).
[8] Y. R. Shen, Liq. Cryst. **5**, 635 (1989).
[9] M. B. Feller, W. Chen, and Y. R. Shen, Phys. Rev. A **43**, 6778 (1992).
[10] M. Barmentlo, R. W. J. Hollering, and N. A. J. M. van Aerle, Liq. Cryst. **14**, 475 (1993).
[11] B. Jerôme and Y. R. Shen, Phys. Rev. E **48**, 4556 (1993).
[12] K. Shirota, K. Ishikawa, H. Takezoe, A. Fukuda, and T. Shibashi, Jpn. J. Appl. Phys., Part 2 **34**, L316 (1995).
[13] K. Shirota, M. Yaginuma, T. Sakai, K. Ishikawa, H. Takezoe, and A. Fukuda, Appl. Phys. Lett. **69**, 164 (1996).
[14] B. Park, H.-H. Choi, H. S. Kim, H.-K. Hwang, J.-G. Lee, Y.-K. Kim, H.-S. Woo, C. S. Jung, Y. H. Park, M. H. Choi, Y. S. Kim, M. Kakimoto, and H. Takezoe, J. Korean Phys. Soc. **30**, 202 (1997).
[15] B. Park, H. S. Kim, J.-Y. Bae, J.-G. Lee, H.-S. Woo, S. H. Han, J. W. Wu, M. Kakimoto, and H. Takezoe, Appl. Phys. B: Lasers Opt. **66**, 445 (1998).
[16] T. Sakai, J. G. Yoo, Y. Kinoshita, K. Ishikawa, H. Takezoe, A. Fukuda, T. Nihira, and H. Endo, Appl. Phys. Lett. **71**, 2274 (1997).
[17] J.-G. Yoo, H. Hoshi, T. Sakai, K. Ishikawa, H. Takezoe, and Y. S. Lee, J. Appl. Phys. (to be published).
[18] B. Park, Y. Kinoshita, T. Sakai, J.-G. Yoo, H. Hoshi, K. Ishikawa, and H. Takezoe, Phys. Rev. E. **57**, 6717 (1998).
[19] J. J. Maki, M. Kauranen, and A. Persoons, Phys. Rev. B **51**, 1425 (1995).
[20] M. Kauranen, J. J. Maki, T. Veriest, S. V. Elshocht, and A. Persoons, Phys. Rev. B **55**, R1985 (1997).
[21] F. Geiger, R. Stolle, G. Marowsky, M. Palenberg, and B. U. Felderhof, Appl. Phys. B: Lasers Opt. **61**, 135 (1995).
[22] J.-G. Yoo, B. Park, T. Sakai, Y. Kinoshita, H. Hoshi, K. Ishikawa, and H. Takezoe, Jpn. J. Appl. Phys., Part 1 **37**, 4124 (1998).